Efficiency Maps of Electrical Machines: A Tutorial Review

Emad Roshandel, *Student Member, IEEE,* Amin Mahmoudi, *Senior Member, IEEE,* Solmaz Kahourzade, *Member, IEEE,* and Wen L. Soong, *Senior Member, IEEE*

***Abstract*— Efficiency maps (EffMs) illustrate the maximum efficiencies of electric machines over a range of torque-speed operating points. This paper reviews the available techniques for efficiency map calculation and gives a general understanding of EffM modelling and interpretation for traction motors. It shows the accuracy versus calculation effort trade-off for different methods. The process of efficiency map calculation for sample induction motor and permanent magnet synchronous machines is explained. Calculation of EffMs using commercial software is also covered. Finally, possible future research opportunities in this field are suggested.**

***Index Terms*— driving cycles, efficiency maps, electric machines, machine loss, torque speed envelope.**

I. Introduction

EFFICIENCY MAPs (EffMs) project the maximum efficiencies of electric machines (EMs) in the torque-speed (or power-speed) plane [1]. EffMs are widely used to compare the performance of EMs and the torque (or power) versus speed capability (envelope) of the drive system for traction applications. Fig. 1 illustrates the EffM and loss maps of a sample surface-mounted permanent magnet synchronous motor (SPMSM) over a wide range of torque-speed operating points. In addition to efficiency and loss values at each operating point, it shows the maximum achievable torque at any speed including the torque capability at low speeds and the constant power (torque falls inversely with speed) characteristic at higher speeds.

Fig 2 summarizes various methods for obtaining efficiency maps of EMs along with the number of research papers based on about 100 papers published in the last thirty years (1992-2022). It is seen although other methods becoming popular, the main techniques for calculations of the EffMs are experimental, finite element analysis (FEA), and analytical techniques, respectively. The accuracy of experimental setups and FEA [2], the flexibility of FEA and analytical methods [3], and the fast speed of analytical methods [4] are the main reasons for the popularity of these techniques. The focus of this paper is on the experimental, FEA, analytical, and corrected analytical methods.

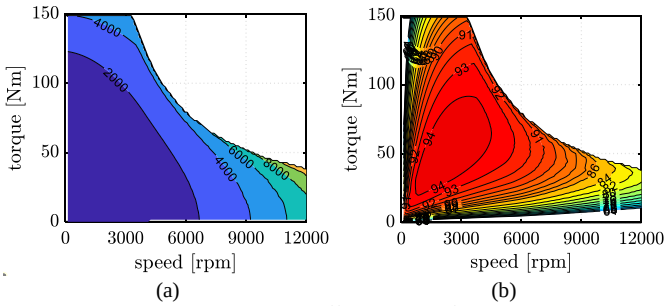

Fig. 1. Example (a) loss map and (b) efficiency map for a 45kW SPMSPM [5].

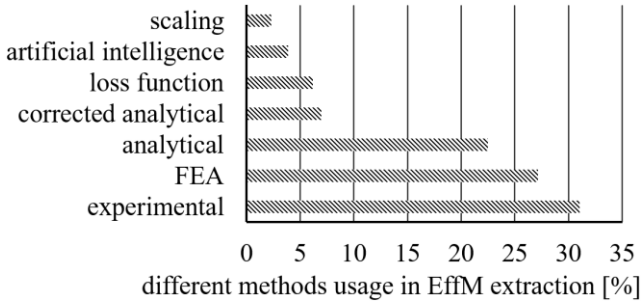

Fig. 2. Summary of the frequency of different approaches used to calculate EffMs based on 100 papers in the period 1992-2022 (data collected by authors).

The calculation of the EffM using scaling techniques [6]–[8] and artificial intelligence [9]–[11] is employed in a few papers. The scaling technique uses the EffM of a certain geometry to estimate the EffM of scaled machines. These methods are generally not reliable when the shapes and material types of some parts of a motor like rotor bar, magnets, and winding structure are changed during the design process. The artificial intelligence-based techniques can avoid this problem if a large data set consisting of the EffM of different geometries and materials are provided. However, the provision of such a data set is generally not possible.

Although there are many papers discussing the EffM, there is a lack of clear steps/guidelines for the calculation of EffM and discussion of the accuracy versus calculation effort trade-off between alternative techniques.

This tutorial/review paper provides a “road map” for engineers and researchers in the field of EM design for transport electrification. It investigates the calculation of efficiency maps

Corresponding Author: Emad Roshandel. This work was supported by the Australian Research Council Discovery under Grant DP170103343.

E. Roshandel is with the College of Science and Engineering at Flinders University, Adelaide, Australia (e-mail: emad.roshandel@flinders.edu.au).

A. Mahmoudi is with the College of Science and Engineering at Flinders University, Adelaide, Australia (e-mail: amin.mahmoudi@flinders.edu.au).

S. Kahourzade is with the STEM at University of South Australia, Adelaide, Australia (e-mail: solmaz.kahourzade@unisa.edu.au).

W. L. Soong is with the School of Electrical and Electronic Engineering, University of Adelaide, Adelaide, Australia (e-mail: wen.soong@adelaide.edu.au).

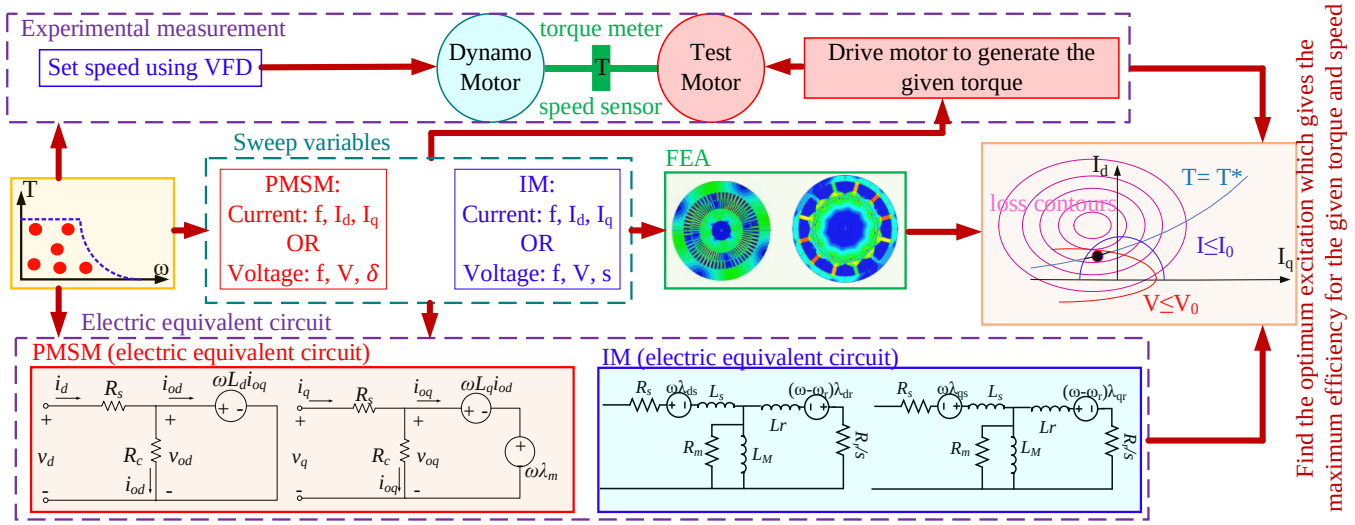

Fig. 3. The general process of the calculation of efficiency maps based on the equivalent circuit, FEA, and experimental measurements.

for AC electric machines and has the following areas of contribution:

- gives a brief tutorial of alternative EffM calculation methods and discusses their trade-offs;
- describes past research on EffMs and identifies research gaps and opportunities for future research.

Section II presents the general concept of the calculation of EffMs. In Section III the different EffM calculation methods for PMSM and induction machine (IM) are described. Section IV describes the direct methods such as experimental approach for the extraction of the EffM. The procedures of EffMs calculation using commercial software are discussed in Section V. In Section VI, the results of the explained methods and software are prepared and compared with each other. Finally, the possible research areas which can help EffM calculation and improve its accuracy are described in Section VII.

II. General Process of Extraction of EffM

The efficiency of the electric motor (η) for a given torque (τ) and speed (ω) is obtained by (1) where the total losses (P_{loss}) of the EM are a function of torque and speed.

$$\eta = \frac{\tau\omega}{\tau\omega + P_{loss}(\tau,\omega)} \quad (1)$$

Normally the efficiency map is defined in terms of the maximum efficiency (or minimum loss) for each torque/speed operation point. In some literature, the EffMs have been calculated based on the maximum torque per ampere (MTPA) control [12]–[14] which corresponds to the minimum stator current and stator winding loss. The MTPA operating points do not necessarily match with the maximum efficiency points especially in the field weakening region. The results of the consideration of these two different control techniques are discussed in this paper. Other efficiency map definitions are also possible such as minimum copper loss or minimum iron loss.

There are multiple ways for obtaining the EffMs of electric machines. These can be classified firstly in terms of their approach:

- experimental methods
- equivalent-circuit approaches
- finite-element analysis

Fig. 3 shows the process of the measurement and calculation of the EffMs using the experimental, FEA, and equivalent circuit calculation methods. Accordingly, Table I summarizes the general steps toward calculation of EffMs. It is seen depending on the considered type of excitation in FEA and electric equivalent circuit modelling, the sweep variables are chosen. For instance, the sweep variable for the voltage-driven PMSM and induction motor (IM) are the power angle (γ) and slip frequency (sf_s), respectively. For a current driven PM and IM, the sweep variables are current (I) and current angle (δ). For a given torque and speed, the loss and efficiency of the motor are obtained through an iterative procedure at different sweep values. The efficiency of the motor in each iteration is recorded when the voltage and current limits are met. Among the collected efficiency values for each torque-speed point, the value which offers the highest efficiency (or smallest loss) is selected to plot the EffM.

TABLE I. General Process of Calculation of EffMs

1. **Determine the sweep variables based on the considered power source and type of EM**
   - For synchronous EM, the sweep parameters are either (V and γ) or (I_d and I_q) or (I and δ).
   - For IM, the sweep variables are (V and sf_s) or (I_d and I_q) or (I and δ).
2. **Create torque and speed matrices**
   - Create a matrix in the range of the minimum and maximum values for torque and speed.
   - Select one torque (τ) and speed (ω) point for calculation.
3. **Calculate efficiency for a given pair of torque and speed**
   - Vary one of the sweep parameters over a range.
   - For the given τ and ω, find the values of the other sweep variable.
   - Find the maximum efficiency while meeting voltage and current constraints.
4. **Report the efficiency at the minimum loss point (i.e., maximum efficiency)**

As shown in Fig. 3, the experimental test follows a similar process where the given speed is set by the dynamo motor drive. The test motor drive works on the torque control mode while it can use voltage-driven or current driven control method to find the maximum efficiency point for each pair of τ and ω.

It also possible to classify efficiency maps methods as:

- indirect methods: torque is predicted, usually from flux-linkage, losses are predicted using a simplified model, such as the iron loss is only a function of speed. This can be done using equivalent-circuit or finite-element methods.
- direct methods: torque and losses are directly predicted or measured. This can be done using finite-element or experimental methods.

The calculation and experimental procedures will be explained in details in the next two sections.

III. Indirect Efficiency Map Estimation

A. Principles

When explaining the principles of indirect efficiency map calculation using equivalent circuits it is useful to consider a synchronous machine driven by *d*- and *q*-axis currents (I_d, I_q). It is desired to find the corresponding *dq*-axes flux linkages (λ_d, λ_q). These allow calculating the torque (τ) given the number of phases *m* and pole-pairs *p*,

$$\tau = mp\left(\lambda_d I_q - \lambda_q I_d\right) \tag{2}$$

From the stator resistance R_s and the electrical frequency ω_e the *dq*-axes voltages can be found,

$$\begin{aligned} V_q &= R_s I_q + \lambda_d \omega_e \\ V_d &= R_s I_d - \lambda_q \omega_e \end{aligned} \tag{3}$$

The stator current *I* and voltage *V* are thus given by,

$$I = \sqrt{I_d^2 + I_q^2} \quad \text{and} \qquad V = \sqrt{V_d^2 + V_q^2} \tag{4}$$

When calculating efficiency maps, the selected operating point must meet the requirement that both the current and voltage are within the rated current I_0 and rated voltage V_0,

$$I \le I_0 \quad \text{and} \quad V \le V_0 \tag{5}$$

The stator copper losses are given by,

$$P_{cu} = mI^2 R_s \tag{6}$$

There are three methods for obtaining the *dq*-axes flux linkages [15]:

- linear: $\lambda_d(I_d)$ and $\lambda_q(I_q)$ where the functions are linear (see the red lines in Fig. 4) which correspond to constant values for the inductances L_d and L_q
- saturation: $\lambda_d(I_d)$ and $\lambda_q(I_q)$ where the functions are non-linear (see the black lines in Fig. 4) due to magnetic saturation, this corresponds to varying inductances $L_d(I_d)$ and $L_q(I_q)$
- cross-saturation: for highly saturated electric machines it can be necessary to consider cross-saturation where I_q affects λ_d, and hence $\lambda_d(I_d, I_q)$ and similarly $\lambda_q(I_d, I_q)$. Thus, $L_d(I_d, I_q)$ and $L_q(I_d, I_q)$. This phenomenon for an interior permanent magnet synchronous machine (IPMSM) is shown by cyan dot-points in Fig. 4.

B. Synchronous Machine Equivalent Circuit Models

Equivalent circuits can be used with the linear, saturation, and cross-saturation flux-linkage/inductance models.

The equivalent circuit for IPMSMs has the following relationships,

$$\begin{aligned} \lambda_d &= \Psi_m + L_d I_d \\ \lambda_q &= L_q I_q \end{aligned} \tag{7}$$

Thus, the main equivalent-circuit parameters are the stator resistance (R_s), PM flux linkage (Ψ_m), and the *dq*-axis inductances (L_d and L_q). These equivalent circuit parameters can be found:

- analytically or from finite-element analysis: based on stator and rotor dimensions, lamination and permanent magnet properties, stator winding information etc.
- experimentally: resistance, inductance/flux-linkage measurements in either stationary or rotating conditions.

These equivalent-circuit parameters can then be used with the equivalent circuit to estimate the flux-linkage from (7) and hence torque and voltage using (2) and (3). From this, the efficiency map can be found.

When using equivalent circuits, the stator iron losses (P_{fe}) can be estimated as a function of speed using an open-circuit test ($P_{oc}(\omega)$). It is done using either finite-element analysis or experimental testing. For the latter this will also include mechanical losses P_{mech} such as friction and windage losses [16], [17]. The total loss $P_{loss} = P_{cu} + P_{fe} + P_{mech}$ is used to find the efficiency (η) by (1).

In the equivalent circuit, the stator iron losses can be approximated as only a function of speed $P_{fe} = P_{oc}(\omega)$ and is often subtracted from the output torque. Alternatively, the stator iron loss is modelled as a parallel resistance in the equivalent circuit and hence as an increased electrical input power.

Fig. 5 illustrates the general process for obtaining efficiency maps using either equivalent circuit or FEA. According to this figure, the following steps should be investigated to find the EffM of a synchronous machine:

- The first step is to identify the operating limits. The rated voltage V_O and current I_O are given. For synchronous machines there are two control variables (I_d, I_q) and for conventional PM and reluctance machines, the normal ranges are presented in (8).

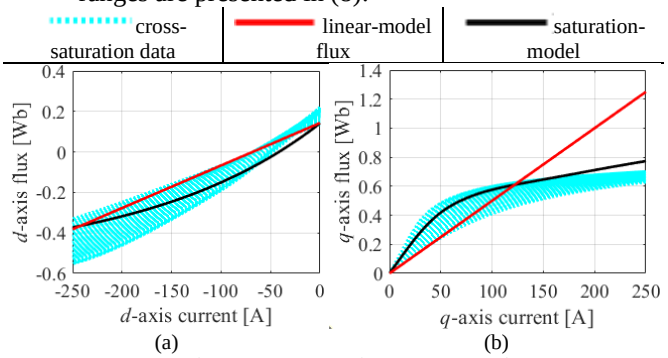

Fig. 4. The variation of *d*-axis and *q*-axis flux vs. current of a IPMSM studied in [18]. (a) The *d*-axis flux variation. (b) The *q*-axis flux variation.

$$-I_0 \le I_d \le 0 \quad \text{and} \quad 0 \le I_q \le I_0 \tag{8}$$

- Secondly, matrices of torque and speed operating points covering the desired operating range (τ,ω) are generated, given the operating speed (ω), the electrical frequency ($\omega_e = p\omega$).
- Thirdly, for each operating point, a vector of (negative) d-axis current (I_d) points in the allowable range given by (8) is considered. Eqs. (2) and (7) are used to identify the required (positive) q-axis current values (I_q) to generate the required torque. From these the corresponding total current, voltage, losses, and hence efficiency are determined. This allows finding the maximum efficiency for that operating point, within the required current and voltage constraints in (5). This is repeated for all operating points to find the efficiency map.

C. Finite-Element Mapping

A more accurate means for efficiency map calculation, particularly for highly saturated machines, is to avoid using the approximations associated with the equivalent circuit in (7) and instead directly use the flux-linkage $\lambda_d(I_d, I_q)$ and $\lambda_q(I_d, I_q)$. Generally, a large number of finite-element simulations is used to create flux-linkage "maps" of λ_d and λ_q on the (I_d, I_q) plane. In [19], a 15×15 mesh of (I_d, I_q) points were used. The flux-linkage maps can also be found experimentally. As illustrated in Fig. 5, for a given (I_d, I_q) the flux maps are used to find λ_d, λ_q, and hence find torque and voltage using (2) and (3).

Similarly, to the flux-linkage maps, maps of the stator hysteresis, stator eddy-current, and rotor magnet eddy-current loss maps are found in the (I_d, I_q) plane at a reference speed ω_0 using finite-element analysis. Then, for given values of (I_d, I_q) and the actual speed (ω), actual losses can be found by scaling the loss map results appropriately [20],

$$\begin{aligned} P_{hys}(I_d, I_q, \omega) &= P_{hys}(I_d, I_q, \omega_0) \cdot (\omega/\omega_0) \\ P_{eddy}(I_d, I_q, \omega) &= P_{eddy}(I_d, I_q, \omega_0) \cdot \left(\frac{\omega}{\omega_0}\right)^2 \end{aligned} \tag{9}$$

D. Induction Machine Efficiency Maps

A similar process shown in Fig. 5 can be used for induction machines. For induction machines, the equivalent circuit has three inductances, the magnetising inductance (L_m), the stator leakage inductance (L_{ls}), and the referred rotor leakage inductance (L'_{lr}). From these, the stator and rotor inductances can be defined as $L_s = L_m + L_{ls}$ and $L_r = L_m + L'_{lr}$. These values can be found analytically [21], from finite-element analysis [22], or experimentally [23].

For induction machines, the dq-axes fluxes are estimated using (10) knowing the machine dq-axes inductances.

$$\begin{cases} \lambda_d = L_d I_d; \text{where } L_d = L_s \\ \lambda_q = L_q I_q; \text{where } L_q = (L_s - \dfrac{L_m^2}{L_r}) \end{cases} \tag{10}$$

The torque is estimated using (2). The stator electrical frequency (ω_e) is required to obtain the stator voltage using (3). As shown in (11), the value of ω_e depends on slip speed (ω_{slip}).

$$\omega_e = p(\omega + \omega_{slip}) \tag{11}$$

where the slip speed is defined in terms of the referred rotor resistance $R_r{}'$ and rotor inductance (L_r) [24],

$$\omega_{slip} = \frac{R_r{}' I_q}{L_r I_d} \tag{12}$$

For induction machines, the typical operating values of slip speed is between zero and the value corresponding to maximum torque, $\omega_{slip(Tmax)}$,

$$\omega_{slip(Tmax)} = \frac{\omega_s R'_2}{|R_1 + j\omega_s(L_{ls} + L'_{lr})|} \tag{13}$$

where $\omega_s = 2\pi f_s/p$ is the rated synchronous speed with rated supply frequency f_s.

For each torque-speed operating point, a range of slip speeds in the above range is considered and the corresponding values of I_d and I_q are determined using (2), (10) and (12). Then, the voltage, ohmic loss, and core loss are calculated. The core loss is modelled as a parallel resistance, and the ohmic loss including the stator winding and rotor cage losses is modelled by series resistances in the equivalent circuit. Based on this, the maximum efficiency for the torque-speed points, while meeting the voltage and current constraints in (5), can be found.

For induction machines, the saturation of the magnetising inductance (L_m) is important to consider. It is normally modelled as a function of the magnetising current (I_m) and this can be determined by a no-load test in either finite-element analysis or experimental testing.

The rotor resistance can also depend on the slip frequency due to deep bar effects [25]. This dependency can be found using locked-rotor tests at different slip speeds (either using finite-element analysis or experimental tests) [26].

E. Voltage Control vs Current Control

Variable-speed electric machines are normally current-controlled using a field-oriented control technique. It allows rapid control of instantaneous torque and fast over-current protection. This technique is generally less sensitive to motor parameter variations at low speeds. On the other hand, line-operated machines are inherently voltage controlled. Voltage control is simpler to implement while over-current protection is more difficult. It is simpler to control during high-speed field-weakening operation but has generally poorer dynamics.

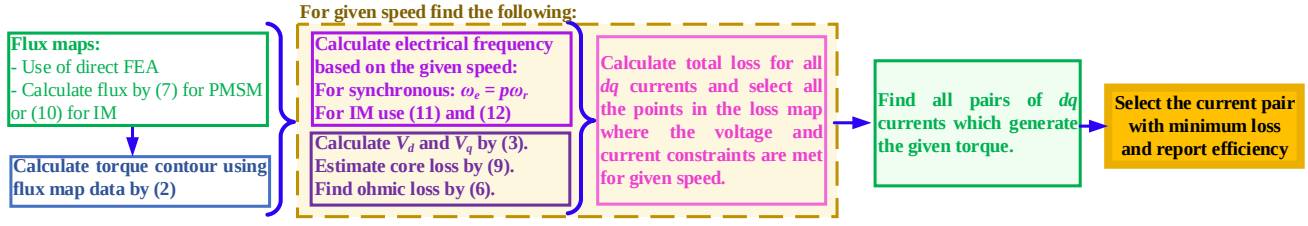

Fig. 5. The summary of procedure of the calculation of EffMs using the equivalent circuit for IM and PMSM.

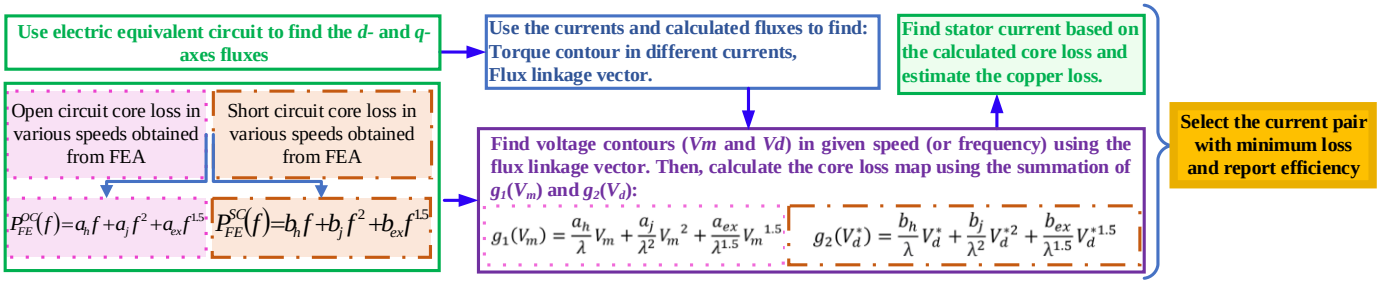

Fig. 6. The computationally efficient FEA approach for efficiency map calculation of PMSMs. Magnetising and demagnetising voltages are shown by V_m and V_d, respectively. The flux linkage is shown by λ.

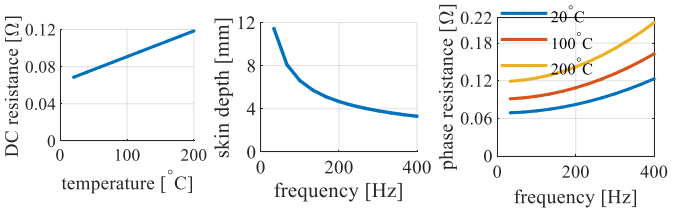

Fig. 7. The temperature and frequency variation effects on the resistance of the winding of the studied IPMSM. (a) the resistance variation vs. temperature, (b) reduction of the effective area of a wire due to the skin effect by increment of the frequency, (c) resistance variation by temperature and frequency.

For voltage control of synchronous machines normally the voltage magnitude $V$and power angle γ between the voltage and the q-axis (which is the back-emf for permanent magnet machines). This defines the dq-axis voltages as,

$$V_q = V\cos\gamma \quad \text{and} \quad V_d = -V\sin\gamma \tag{14}$$

If magnetic saturation and stator resistance is neglected, then (3) and (7) can be used to find a closed-form solution for the dq-axis currents. However, in general, an iterative approach is required to solve for the dq-axis currents. For voltage control of induction machines, normally the slip (s) or slip frequency (sf_s) is used instead of the rotor angle.

F. Core Loss Models

At higher speeds, EM core losses become more significant. They also affect the stator current and so cause a small increase in the winding losses [17]. The induction machine core loss modelling was discussed in [27]. In [27], authors introduced an iron loss scaling technique. This model is used to update the Foucault eddy current loss obtained from a single frequency and scaled it to find iron loss in other frequencies.

In [28], an improved analytical core loss model based on the short circuit and open circuit characteristics of the PM motors was proposed. The approach is summarized in Fig. 6. It is seen that the stator iron loss is considered the superposition of the loss from the main magnetizing flux and from the PM flux. The main magnetising flux is related to the magnetising voltage (V_m) which is the induced stator voltage, and this loss is found from the open-circuit test. The PM flux is directly related to the demagnetising voltage (V_d) and this loss is found from the short-circuit test. This method is more accurate than the simple equivalent circuits for the calculation of efficiency in both rated flux and field-weakening operating regions. It was later improved by including saturation and cross-saturation effects [29].

G. Effect of Temperature

Temperature can significantly affect the efficiency of an electric machine. As shown in (15) and Fig. 7a, the resistance of windings has a direct relationship with temperature [30].

$$R = R_{ref}\left(1 + \alpha\left(\theta - \theta_{ref}\right)\right) \tag{15}$$

In (15), the reference resistance (R_{ref}) is the value of the resistance measured at reference temperature (θ_{ref}). The temperature coefficient of the material is shown by α; and θ is the average temperature of the conductors. The temperature co-efficient of copper is about 0.39%/°C which means that, for instance, a 100°C temperature rise would result in a 39% increase in the stator winding resistance and hence losses. In a similar fashion the temperature co-efficient of resistance of aluminium (0.40%/°C) needs to be considered in the rotor resistance of induction machines. In addition, the increase in temperature also increases the resistivity of the permanent magnets which will generally increase the rotor magnet losses.

The properties of permanent magnets are significantly affected by temperature including their remanent flux density B_r, their coercivity H_c and their demagnetisation knee point [31], [32]. This causes the PM flux linkage Ψ_m of PM machines to reduce significantly with temperature resulting in the torque reduction and copper losses increase at higher temperatures. For instance, the temperature co-efficient of the commonly used NdFeB rare-earth magnet material is typically in the range -0.45 [33] to -0.65%/°C and hence a 50°C temperature increase will reduce the PM flux linkage and hence PM torque by about 25-30%.

Iron losses of lamination materials generally reduce slightly with temperature partially due to the increase in the resistivity of the material reducing the eddy-current losses [34]. For example, for a particular lamination material at 1,000 Hz [35], the iron loss reduced by about 10% for a 60°C increase in temperature which corresponds to a temperature co-efficient of about -0.2%/°C.

For machines using rolling-element bearings, temperature substantially affects the grease viscosity and hence bearing losses [36].

For equivalent-circuit and finite-element-based efficiency map estimation, it is useful to have estimates of the operating temperatures in the machine either from design information or from a reliable thermal model.

H. AC Winding Loss Effects

The resistance of the winding also increases with frequency due to the skin effect (see Fig. 7b). Increasing frequency

reduces the skin depth and hence the effective area of the wire. This can be modeled using the skin effect equation [37] to improve the accuracy of the ohmic loss estimation. Fig. 7c shows the variation of the equivalent resistance of a sample phase winding at different temperatures and frequencies.

In addition to skin effect, another frequency related winding loss is called proximity effect. This is associated with AC losses in a conductor due to it being exposed to magnetic fields created by AC currents flowing in other nearby conductors [38].

The above effects can be modelled to a first approximation by a stator resistance which is a function of frequency.

I. Effect of Inverter Harmonics

Analytical and FEA methods generally assumes sinusoidal voltages. The core loss increases when an EM is supplied by inverter due to the injection of high order harmonics. Inverter voltage harmonics increase the ohmic loss (i.e., skin and proximity loss) in induction motors and the eddy current PM loss in PM machines.

The electric equivalent circuit models can be solved for different harmonics of the inverter when the amplitude of the harmonics is determined analytically. These methods are not accurate because the equivalent circuit parameters are found based on the fundamental frequency [39]. The inverter harmonics can be modelled in FEA by coupling a circuit simulator with the FEA or use of predefined inverter waveforms [40]. However, these approaches substantially increase the simulation time. An analytical model considering the effect of the high-order harmonics for correct estimation of the conductive, core, and PM losses is complex and yet to be presented.

IV. Direct Efficiency Map Estimation

In a direct method for estimation of EffMs, torque, voltage, and losses are directly found for the operating condition (I_d, I_q, ω). It can be performed using either:

- finite-element analysis: a simulation model is run at the operating conditions and the finite-element predictions of torque, voltage and losses are used.
- experimental testing: a prototype machine is run on a dynamometer at the operating conditions and the measurements are taken for voltages, currents, input and output power.

These direct efficiency map results are more accurate than indirect estimation methods but are slower and for experimental measurements requiring a prototype machine and significant experimental equipment.

As shown in Fig. 3, experimental measurement of the efficiency map of a test machine involves loading it with a dynamometer machine and finding its minimum input power when producing each desired torque and speed operating point.

Both the test and load machines need to be controlled by variable-frequency drives. One drive is normally in speed control mode and the other in torque control mode to allow stable operation. The test machine generally acts as a motor and the dynamometer machine as a generator. The generated power can be dissipated in a resistive load bank or regenerated to the AC mains. A more efficient approach is to connect the DC link of the two drives together to allow recirculation of the power. This means that the only input power required is that to supply losses in the system.

An electric power analyzer is normally used to measure the voltage, current, and power at the input of the test motor. A brushless torque transducer allows measurement of the torque and speed signals. For synchronous machines, the stator current frequency can also be used for speed estimation.

The measurement of the EffMs can be carried out using a hardware in the loop (HIL) system [41]–[43]. In such a system, the collection of the measured data and setting the drive torque-speed references is done using devices like field-programmable gate array (FPGA) boards [44] or general purpose control hardware such as a dSPACE MicroLabBox [23].

There are two approaches when experimentally measuring the efficiency for a given operating point. Firstly, searching for the optimum (I_d, I_q) within the voltage and current constraints, likely starting from a pre-calculated optimum reference (I_d, I_q) value found using analytical or numerical methods. Secondly, just applying the pre-calculated reference values, checking that the torque is achieved and voltage/current limits are maintained, and then measuring the efficiency [23].

The number of torque-speed operating points required for an accurate efficiency map calculation has been investigated. One researcher used 1,600 operating points [45], while a later work indicated that 300 operating points may be sufficient for calculation of an EffM up to 5 times of the rated speed [42].

In an standard efficiency measurement process [43], [45], data should normally be collected at a constant temperature. At the start of the test the machine is normally loaded at the rated torque allowing to reach its rated temperature. During the EffM measurement process, the loading can be varied to seek to maintain the motor temperature within acceptable limits [43].

V. Calculation of EffMs using Commercial Software

Commercial finite-element software such as Ansys Electromagnetics [46], JMAG [47], and Motor-CAD [48] have introduced toolboxes to calculate the EffMs of the EMs. In this section, the methods that these toolboxes use to calculate EffMs are briefly explained.

These toolboxes compute the fluxes and losses over a range of current magnitudes and current angles for PM machines. A process similar to that described in Section III.C is then used to find the EffMs. Where JMAG and Ansys electromagnetics use a complete FEA to find these data, motor-CAD uses a combination of FEA and an analytical solver to build the loss maps of the EMs [49]. Hence, the EffM calculation time of the motor-CAD is less than the others. JMAG and motor-CAD use the current-driven model to predict the EffM of induction machines. Ansys electromagnetic uses a voltage-driven model for induction machine EffM calculation. In this model, the voltage magnitude, slip, and frequency are variables.

Ansys Electromagnetics offers various control methods including minimum total loss, MTPA, minimum copper loss, or minimum iron loss. Stator current control ($I_d = 0$), MTPA, maximum torque per flux, and maximum efficiency are the available control methods provided by JMAG. MotorCAD only reports the EffMs calculated by MTPA control.

These toolboxes use a similar approach to consider the additional loss factors. The resistance values are updated analytically before loss calculation in these packages. The skin and proximity effects on stator resistance can be considered. However, these effects are applied analytically to update the losses. The mechanical losses are based on a user-defined input. These toolboxes ignore the effect of the inverter harmonics for loss computation.

VI. Discussion on EffMs Calculation Models

This section discusses EffMs of induction and permanent magnet motors and compares the results of different methods with consideration of the various factors in EffMs calculation.

A. *EffM of IMs*

This section compares the calculated efficiency maps for an example 2.2kW IM investigating the effects of using linear versus saturation models and maximum efficiency versus MTPA control. The studied IM electrical characteristics and geometry are tabulated in Appendix I.

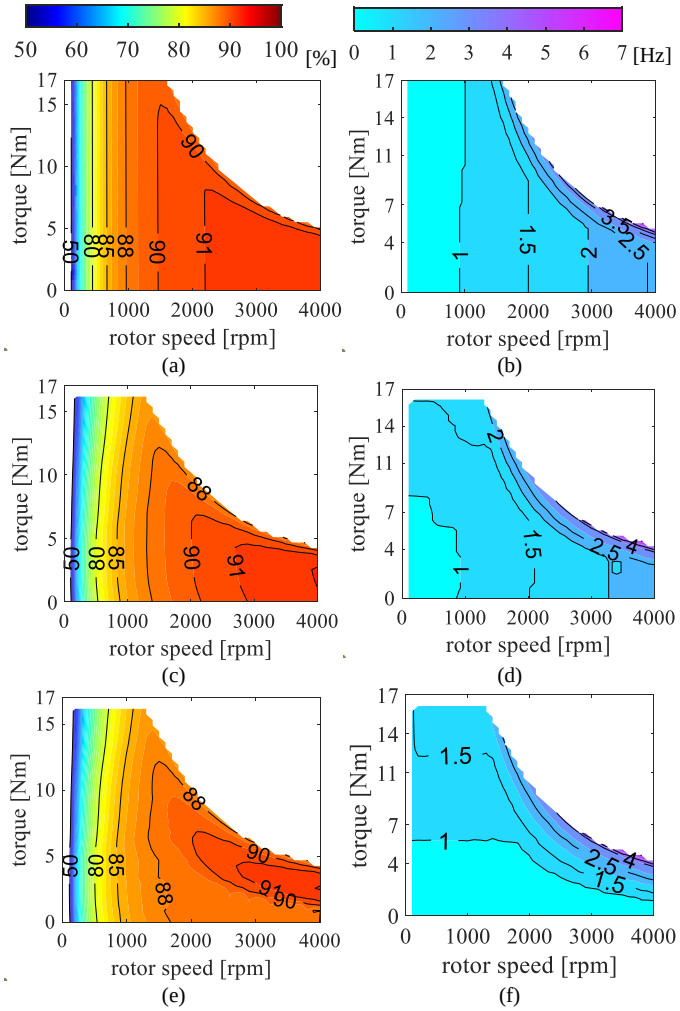

Fig. 8. The calculated efficiency maps (left column) and corresponding required control parameter of slip frequency (right column) for an example 2.2kW IM based on the equivalent circuit model. Rows 1 and 2 are using a linear (Row 1) and saturating (Row 2) magnetizing inductance with maximum efficiency control. Row 3 is using a saturating model but with MTPA control.

Fig. 8 shows calculated efficiency maps (first column) and corresponding required control parameter of slip frequency (second column) for three cases based on the equivalent circuit model. The first two rows use maximum efficiency control with row 1 showing a constant (equal to its rated value) magnetising inductance and row 2 including saturation. Row 3 uses MTPA control and includes saturation.

The effect of magnetising inductance saturation (comparing rows 1 and 2), is to slightly reduce the low-speed torque capability, reduce the efficiency over most of the operating range and to increase the required slip frequency at higher torques in the low-speed region. The effect of MTPA versus maximum efficiency control (comparing rows 2 and 3) is a small reduction of efficiency at low to medium torque values at higher speeds with a significantly different slip frequency used.

In some literature and commercial software, like Motor-CAD [48], MTPA control is used to calculate the EffM instead of the maximum efficiency control. The obtained EffM from Motor-CAD software for the same 2.2kW induction machine is presented in Fig. 9 and shows a good agreement with the equivalent-circuit results with MTPA (Fig. 8e).

B. *EffM of PMSMs*

The efficiency map of a 50kW interior permanent magnet motor (i.e., 2nd generation IPMSM in [18]) is presented in Fig. 10. Several 2-D FEA simulations are executed to find the equivalent circuit parameters with and without saturation consideration. Also, the *dq*-fluxes required for the flux mapping technique are obtained in different pairs of *dq*-currents using 2-D FEA.

Comparison of the efficiency map calculated with the linear electric equivalent circuit (Fig. 10a) and with consideration of the saturation (Fig. 10b) shows the smaller efficiency of the machine in the constant torque region and a higher efficiency in the field weakening region. A constant value of the core resistance in the electric equivalent circuit was considered to estimate the core losses in the linear model. The Steinmetz equation was used for core loss prediction in the saturation model. In Fig. 10(c), the core losses were estimated using the corrected analytical model with FEA explained in Section III.C and Fig. 6. It is seen that the obtained efficiency map using this technique is mostly like the linear model since the inductances are constant in the performance estimation.

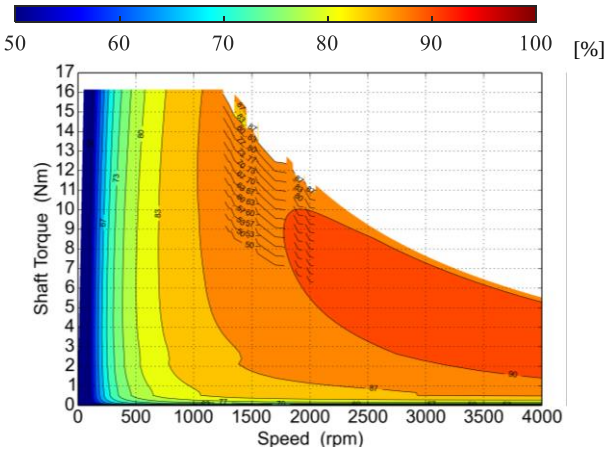

Fig. 9. Efficiency maps of the 2.2kW IM obtained by MotorCAD using MTPA control.

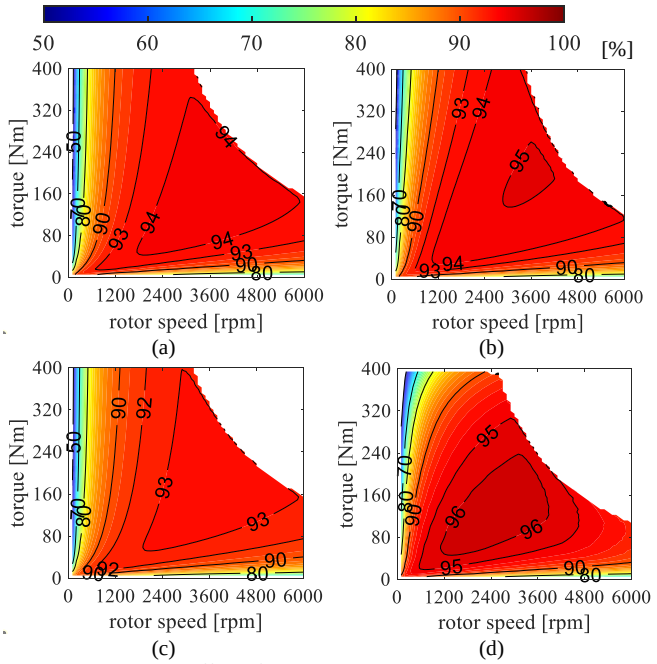

Fig. 10. Calculated EffM of a 50kW IPMSM using (a) linear electric equivalent circuit, (b) including saturation model, (c) corrected core loss approach with electric equivalent circuit. (d) flux mapping technique.

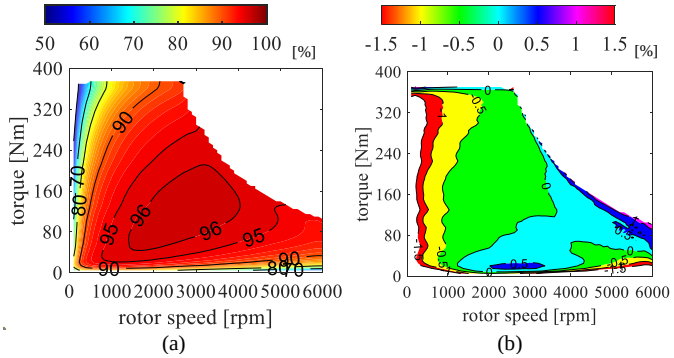

Fig. 11. The calculated efficiency map of the considered IPMSM using (a) Ansys Electromagnetics and (b) its difference by the flux mapping method.

TABLE II. COMPARISON OF THE CLASSICAL METHODS IN TERMS OF ACCURACY AND SPEED OF CALCULATION FOR AN EXAMPLE ANALYSIS.

Methods	Max error %	FE Simulations	FE simulations time	Calculation time
Linear equivalent circuit	20%	2	0.17 h	0.01 m
Saturation equivalent circuit	10%	41	3.7 h	0.38 m
Corrected core loss	15%	80	7.4 h	0.87 m
Flux mapping technique	1.5%	225	19 h	0.6 m
Ansys Electromagnetics	0%	500	43 h	4 m

The flux mapping technique is used to calculate the EffM in Fig. 10d, the maximum torque in the constant torque region is slightly reduced due to the *q*-axis flux reduction at higher currents. The flux-linkage results for this machine were given earlier in Fig. 4 which shows when the *d*-axis current is zero and *q*-axis current is at its maximum value, the *q*-axis flux is less than the saturation model and the linear electric equivalent circuit. As shown in Fig. 4, the *d*-axis flux reduces significantly at larger currents in comparison to the linear and saturation models. This reduction on one hand leads to reduction of the efficiency because of the increase of the core losses in the field weakening region. On the other hand, it limits the torque generation. As shown in Fig. 10d, at the end of the field weakening region, the obtained torque is less than the saturation and linear models.

Table II compares the above EffM calculation techniques in terms of accuracy and time. The accuracy is reported based on the comparison of the results in Fig. 10 with the FEA predicted efficiency maps from Ansys Electromagnetics [46]. In this table, the simulation time for the linear equivalent circuit is the time for running open-circuit and short-circuit FEA simulations to find the equivalent circuit parameters. The time for the saturation equivalent circuit includes the FEA simulation times for loading tests at 40 points to find the *d*- and *q*-axis inductances and an open-circuit test to find the core loss value. The time for the corrected core loss models includes 40 open-circuit and 40 short-circuit FEA simulations at different operating speeds to find the core loss variation. Finally, the flux mapping technique preparation time covers the collected data for 15×15 pairs of *d*- and *q*-axis currents to find the flux and loss maps. The required simulation time is an important factor for selection of the method in each application. In this table, the calculation time is the required time for estimation of EffM for all considered pairs of torque and speed.

The calculated EffM from the Ansys Electromagnetics and its difference with the results of the flux mapping technique are presented in Figs. 11a and 11b, respectively. A comparison of Figs. 10d and 11a shows that the maximum produced torque in the constant torque region is about 5% less than the flux mapping technique. The difference map shown in Fig. 11b demonstrate these two methods have less than 1.5% efficiency difference in the torque-speed envelope.

VII. RESEARCH OPPORTUNITIES

Although many studies on the calculation of the efficiency maps have been conducted, some aspects of the losses have not been studied in detail. For instance, in most of the calculation methods, the converter losses which play an important part especially at higher speeds have been ignored. It has been shown that the converter losses can be equal to the core losses at higher speeds under light load conditions [50]. Therefore, it is useful to include the effect of this type of loss for EffMs calculation. The inverter operation also leads to injection of high-order harmonics into the winding which can affect the ohmic and core losses of EMs is another important factor to improve the accuracy of the estimated EffM.

It is possible to include the inverter in a multi-physics simulation for analytical and FEA. However, it substantially increases the computation time. The development of an analytical model for calculation of the inverter losses can improve the accuracy of the analytical and combined analytical-FEA calculation of EffMs.

The improvement of the accuracy of the estimation of core loss is another important subject for further study. Although the Steinmetz and Bertotti equations offer good accuracy in the estimation of the core losses, they ignore the effect of high order harmonics, especially in tooth. In addition to the discussed

models, literature has introduced loss function to predict the efficiency maps. However, loss functions do not predict the core losses with an acceptable accuracy [51].

The available temperature effect consideration is usually done based on the machine temperature for a certain operating point. However, the machine temperature changes with the load. As discussed in [52], the challenges of multi-physics simulation using computationally-expensive numerical methods are the main challenges consideration of temperature effects in EffMs. A fast dynamic modelling of the thermal behavior of the machine is useful to update the machine model parameters during a vehicle driving cycle.

VIII. Conclusion

In this paper, various efficiency map (EffM) calculation techniques including their advantages and disadvantages were explained. Also, alternative methods to improve the calculation accuracy/speed of the EffMs were discussed. Finally, possible future research opportunities were highlighted.

Appendix I

TABLE III. STUDIED IM ELECTRICAL CHARACTERISTICS AND GEOMETRY.

Electrical Characteristics			
Rated line voltage [V]	415	Rated power [W]	2200
Frequency [Hz]	50	Number of poles	4
Geometry and dimensions			
Stator outer diameter [mm]	165	Stator inner diameter [mm]	105
Rotor outer diameter [mm]	104	Rotor inner diameter [mm]	38
Number of stator slots	36	Number of rotor slots	28
Lamination material	M19	Stator winding [AWG]	18

References

[1] K. Kiyota, H. Sugimoto, and A. Chiba, "Comparing Electric Motors: An Analysis Using Four Standard Driving Schedules," *IEEE Ind. Appl. Mag.*, vol. 20, no. 4, pp. 12–20, Jul. 2014, doi: 10.1109/MIAS.2013.2288380.

[2] K. Li, S. Han, S. Cui, and A. Bouscayrol, "Sizing of modular cascade machines system for electric vehicles," *IEEE Trans. Veh. Technol.*, vol. 68, no. 2, pp. 1278–1287, 2019, doi: 10.1109/TVT.2018.2886402.

[3] M. H. Mohammadi and D. A. Lowther, "A Computational Study of Efficiency Map Calculation for Synchronous AC Motor Drives Including Cross-Coupling and Saturation Effects," *IEEE Trans. Magn.*, vol. 53, no. 6, 2017, doi: 10.1109/TMAG.2017.2661994.

[4] P. Dück and B. Ponick, "A novel iron-loss-model for permanent magnet synchronous machines in traction applications," *2016 Int. Conf. Electr. Syst. Aircraft, Railw. Sh. Propuls. Road Veh. Int. Transp. Electrif. Conf. ESARS-ITEC 2016*, 2016, doi: 10.1109/ESARS-ITEC.2016.7841432.

[5] A. Mahmoudi, W. L. Soong, G. Pellegrino, and E. Armando, "Efficiency maps of electrical machines," in *2015 IEEE Energy Conversion Congress and Exposition (ECCE)*, Sep. 2015, pp. 2791–2799, doi: 10.1109/ECCE.2015.7310051.

[6] R. B. Sepe, J. M. Miller, and A. R. Gale, "Intelligent efficiency mapping of a hybrid electric vehicle starter/alternator using fuzzy logic," in *Gateway to the New Millennium. 18th Digital Avionics Systems Conference. Proceedings (Cat. No.99CH37033)*, 1999, vol. B.6-6 vol., pp. 8.B.2-1-8.B.2-8, doi: 10.1109/DASC.1999.822007.

[7] J. Sepe, C. M. Morrison, J. M. Miller, and A. R. Gale, "High efficiency operation of a hybrid electric vehicle starter/generator over road profiles," *Conf. Rec. - IAS Annu. Meet. (IEEE Ind. Appl. Soc.*, vol. 2, no. C, pp. 921–925, 2001, doi: 10.1109/ias.2001.955562.

[8] C. T. Krasopoulos, M. E. Beniakar, and A. G. Kladas, "Multicriteria PM motor design based on ANFIS evaluation of EV driving cycle efficiency," *IEEE Trans. Transp. Electrif.*, vol. 4, no. 2, pp. 525–535, 2018, doi: 10.1109/TTE.2018.2810707.

[9] K. Zhou, A. Ivanco, Z. Filipi, and H. Hofmann, "Finite-Element-Based Computationally Efficient Scalable Electric Machine Model Suitable for Electrified Powertrain Simulation and Optimization," *IEEE Trans. Ind. Appl.*, vol. 51, no. 6, pp. 4435–4445, 2015, doi: 10.1109/TIA.2015.2451094.

[10] S. Stipetic and J. Goss, "Calculation of efficiency maps using scalable saturated flux-linkage and loss model of a synchronous motor," *Proc. - 2016 22nd Int. Conf. Electr. Mach. ICEM 2016*, pp. 1380–1386, 2016, doi: 10.1109/ICELMACH.2016.7732704.

[11] S. Stipetic, J. Goss, D. Zarko, and M. Popescu, "Calculation of Efficiency Maps Using a Scalable Saturated Model of Synchronous Permanent Magnet Machines," *IEEE Trans. Ind. Appl.*, vol. 54, no. 5, pp. 4257–4267, 2018, doi: 10.1109/TIA.2018.2837672.

[12] E. Dlala *et al.*, "Efficiency map simulations for an interior PM motor with experimental comparison and investigation of magnet size reduction," in *2013 International Electric Machines & Drives Conference*, May 2013, pp. 23–29, doi: 10.1109/IEMDC.2013.6556124.

[13] B. Dianati, S. Kahourzade, and A. Mahmoudi, "Optimization of Axial-Flux Induction Motors for the Application of Electric Vehicles Considering Driving Cycles," *IEEE Trans. Energy Convers.*, pp. 1–1, 2020, doi: 10.1109/TEC.2020.2976625.

[14] C. Lopez-Torres, C. Colls, A. Garcia, J. R. Riba, and L. Romeral, "Development of a Behavior Maps Tool to Evaluate Drive Operational Boundaries and Optimization Assessment of PMa-SynRMs," *IEEE Trans. Veh. Technol.*, vol. 67, no. 8, pp. 6861–6871, 2018, doi: 10.1109/TVT.2018.2823339.

[15] S. Kahourzade, A. Mahmoudi, W. L. Soong, N. Ertugrul, and G. Pellegrino, "Estimation of PM Machine Efficiency Maps from Limited Data," *IEEE Trans. Ind. Appl.*, vol. 56, no. 3, pp. 2612–2621, 2020, doi: 10.1109/TIA.2020.2979975.

[16] G. Burnand, D. M. Araujo, C. Koechli, and Y. Perriard, "Validation by measurements of a windage losses model for very-high-speed machines," in *2017 20th International Conference on Electrical Machines and Systems (ICEMS)*, Aug. 2017, pp. 1–4, doi: 10.1109/ICEMS.2017.8056273.

[17] K. Li, S. Cui, A. Bouscayrol, and M. Hecquet, "Analytical derivation of efficiency map of an induction machine for electric vehicle applications," *2018 IEEE Veh. Power Propuls. Conf. VPPC 2018 - Proc.*, no. 1, pp. 1–6, 2019, doi: 10.1109/VPPC.2018.860495000.

[18] K. Kiyota and A. Chiba, "Design of switched reluctance motor competitive to 60-kW IPMSM in third-generation hybrid electric vehicle," *IEEE Trans. Ind. Appl.*, vol. 48, no. 6, pp. 2303–2309, 2012.

[19] S. Ferrari, P. Ragazzo, G. Dilevrano, and G. Pellegrino, "Flux-Map Based FEA Evaluation of Synchronous Machine Efficiency Maps," in *2021 IEEE Workshop on Electrical Machines Design, Control and Diagnosis (WEMDCD)*, 2021, pp. 76–81.

[20] M. Popescu, D. M. Ionel, A. Boglietti, A. Cavagnino, C. Cossar, and M. I. McGilp, "A general model for estimating the laminated steel losses under PWM voltage supply," *IEEE Trans. Ind. Appl.*, vol. 46, no. 4, pp. 1389–1396, 2010, doi: 10.1109/TIA.2010.2049810.

[21] E. Roshandel, A. Mahmoudi, S. Kahourzade, and W. L. Soong, "Saturation Consideration in Modeling of the Induction Machine Using Subdomain Technique to Predict Performance," *IEEE Trans. Ind. Appl.*, vol. 58, no. 1, pp. 261–272, Jan. 2022, doi: 10.1109/TIA.2021.3125915.

[22] M. Carbonieri, N. Bianchi, and L. Alberti, "A Fast and Direct Analysis of Three-Phase Induction Motors Using Finite Element," in *2018 XIII International Conference on Electrical Machines (ICEM)*, 2018, pp. 18–24, doi: 10.1109/ICELMACH.2018.8506897.

[23] O. Stiscia, S. Rubino, S. Vaschetto, A. Cavagnino, and A. Tenconi, "Accurate Induction Machines Efficiency Mapping Computed by Standard Test Parameters," *IEEE Trans. Ind. Appl.*, 2022.

[24] M. Carbonieri, N. Bianchi, and L. Alberti, "Induction motor mapping using rotor field-oriented analysis technique," *2019 IEEE Energy Convers. Congr. Expo. ECCE 2019*, pp. 2321–2328, 2019, doi: 10.1109/ECCE.2019.8912787.

[25] H. V. Khang, A. K. Repo, and A. Arkkio, "Resistive loss identification of an inverter-fed deep-bar induction motor," *SPEEDAM 2010 - Int. Symp. Power Electron. Electr. Drives, Autom. Motion*, no. 2, pp. 105–110, 2010, doi: 10.1109/SPEEDAM.2010.5544776.

[26] M. Carbonieri, N. Bianchi, and L. Alberti, "Direct analysis of induction motor using finite element," in *2018 IEEE Energy Conversion Congress and Exposition (ECCE)*, 2018, pp. 277–283.

[27] G. Von Pfingsten, S. Steentjes, and K. Hameyer, "Operating Point Resolved Loss Calculation Approach in Saturated Induction Machines," *IEEE Trans. Ind. Electron.*, vol. 64, no. 3, pp. 2538–2546, Mar. 2017, doi: 10.1109/TIE.2016.2597761.

[28] P. H. Mellor, R. Wrobel, and D. Holliday, "A computationally efficient iron loss model for brushless AC machines that caters for rated flux and field weakened operation," in *2009 IEEE International Electric Machines and Drives Conference*, May 2009, pp. 490–494, doi:

10.1109/IEMDC.2009.5075251.
[29] X. Wu, R. Wrobel, P. H. Mellor, and C. Zhang, "A computationally efficient PM power loss derivation for surface-mounted brushless AC PM machines," in *2014 International Conference on Electrical Machines (ICEM)*, 2014, pp. 17–23.
[30] K. Zhou, J. Pries, and H. Hofmann, "Computationally Efficient 3-D Finite-Element-Based Dynamic Thermal Models of Electric Machines," *IEEE Trans. Transp. Electrif.*, vol. 1, no. 2, pp. 138–149, 2015, doi: 10.1109/TTE.2015.2456429.
[31] K. Selvam and S. Sahoo, "Effect of temperature rise in magnetic materials and deviation of torque in permanent magnet synchronous motor," in *2016 XXII International Conference on Electrical Machines (ICEM)*, Sep. 2020, vol. 2220, no. May 2020, p. 110015, doi: 10.1063/5.0001534.
[32] O. Bilgin and F. A. Kazan, "The effect of magnet temperature on speed, current and torque in PMSMs," in *2016 XXII International Conference on Electrical Machines (ICEM)*, Sep. 2016, no. 1, pp. 2080–2085, doi: 10.1109/ICELMACH.2016.7732809.
[33] C. Lungoci and D. Stoia, "TEMPERATURE EFFECTS ON TORQUE PRODUCTION AND EFFICIENCY OF MOTORS WITH NdFeB," *Rev. Roum. Sci. Techn.-Électrotechn. Énerg*, vol. 53, no. 1, pp. 445–454, 2008.
[34] E. Roshandel, A. Mahmoudi, S. Kahourzade, A. Yazdani, and G. M. Shafiullah, "Losses in efficiency maps of electric vehicles: An overview," *Energies*, vol. 14, no. 22, 2021, doi: 10.3390/en14227805.
[35] Z. Q. Zhu *et al.*, "Evaluation of Iron Loss Models in Electrical Machines," *IEEE Trans. Ind. Appl.*, vol. 55, no. 2, pp. 1461–1472, 2019, doi: 10.1109/TIA.2018.2880674.
[36] G. Du, N. Huang, H. He, G. Lei, and J. Zhu, "Parameter Design for a High-Speed Permanent Magnet Machine under Multiphysics Constraints," *IEEE Trans. Energy Convers.*, vol. 35, no. 4, pp. 2025–2035, 2020, doi: 10.1109/TEC.2020.3000054.
[37] S. Kim and D. P. Neikirk, "Compact equivalent circuit model for the skin effect," in *1996 IEEE MTT-S International Microwave Symposium Digest*, 1996, vol. 3, pp. 1815–1818.
[38] X. Nan and C. R. Sullivan, "An improved calculation of proximity-effect loss in high-frequency windings of round conductors," *PESC Rec. - IEEE Annu. Power Electron. Spec. Conf.*, vol. 2, pp. 853–860, 2003, doi: 10.1109/pesc.2003.1218168.
[39] I. Boldea and S. A. Nasar, *The induction machines design handbook*. CRC press, 2018.
[40] M. Carbonieri, L. DI Leonardo, N. Bianchi, M. Tursini, M. A. Villani, and M. Popescu, "Cage Losses in Induction Motors Considering Harmonics: A New Finite Element Procedure and Comparison with the Time-Domain Approach," *IEEE Trans. Ind. Appl.*, vol. 58, no. 2, pp. 1931–1940, 2022, doi: 10.1109/TIA.2021.3138366.
[41] Y. Loayza, A. Reinap, and M. Alakula, "Performance and efficiency evaluation of FPGA controlled IPMSM under dynamic loading," in *8th IEEE Symposium on Diagnostics for Electrical Machines, Power Electronics & Drives*, Sep. 2011, pp. 550–555, doi: 10.1109/DEMPED.2011.6063677.
[42] R. Bojoi, E. Armando, M. Pastorelli, and K. Lang, "Efficiency and loss mapping of AC motors using advanced testing tools," in *2016 XXII International Conference on Electrical Machines (ICEM)*, Sep. 2016, vol. 1, pp. 1043–1049, doi: 10.1109/ICELMACH.2016.7732654.
[43] G. Haines, N. Ertugrul, and W. L. Soong, "Autonomously obtaining system efficiency maps from motor drive systems," *Proc. IEEE Int. Conf. Ind. Technol.*, vol. 2019-Febru, pp. 231–236, 2019, doi: 10.1109/ICIT.2019.8755199.
[44] G. G. Haines, "Integrated Motor System Estimation Using Efficiency Maps." University of Adelaide, Adelaide, 2020.
[45] K. Stockman, S. Dereyne, D. Vanhooydonck, W. Symens, J. Lemmens, and W. Deprez, "Iso efficiency contour measurement results for variable speed drives," in *The XIX International Conference on Electrical Machines - ICEM 2010*, Sep. 2010, pp. 1–6, doi: 10.1109/ICELMACH.2010.5608035.
[46] "Ansys® Electromagnetics." 2021, [Online]. Available: https://www.ansys.com/academic/terms-and-conditions.
[47] JMAG, "JMAG: simulation technology for electromechanical design." JAPAN, 2021, [Online]. Available: https://www.jmag-international.com/wp-content/uploads/products/pdf/catalog_en.pdf.
[48] Ansys Motor-CAD, "Electric Machine Design Software." 2021, [Online]. Available: https://www.ansys.com/products/electronics/ansys-motor-cad.
[49] T. J. E. Miller and D. A. Staton, *Electric Machine Design using SPEED and Motor-CAD*. Motor Design, 2013.
[50] P. J. Kollmeyer, J. D. McFarland, and T. M. Jahns, "Comparison of class 2a truck electric vehicle drivetrain losses for single- and two-speed gearbox systems with IPM traction machines," pp. 1501–1507, 2016, doi: 10.1109/iemdc.2015.7409261.
[51] A. Mahmoudi, W. L. Soong, G. Pellegrino, and E. Armando, "Loss Function Modeling of Efficiency Maps of Electrical Machines," *IEEE Trans. Ind. Appl.*, vol. 53, no. 5, pp. 4221–4231, Sep. 2017, doi: 10.1109/TIA.2017.2695443.
[52] R. Wrobel, P. H. Mellor, M. Popescu, and D. A. Staton, "Power loss analysis in thermal design of electrical machines," *Proc. - 2015 IEEE Work. Electr. Mach. Des. Control Diagnosis, WEMDCD 2015*, pp. 118–126, 2015, doi: 10.1109/WEMDCD.2015.7194519.